Theor Chem Acc (2002) 107:162–172
DOI 10.1007/s00214-001-0314-x

Theoretical
Chemistry Accounts

Regular article

Monte Carlo simulation of 2-ethoxyethanol in continuum configurational biased procedure: conformational analysis and association in aqueous and non-aqueous media

Mohsen Tafazzoli, Seifollah Jalili

Department of Chemistry, Sharif University of Technology, P. O. Box 11365-9516, Tehran, Iran

Received: 18 January 2001 / Accepted: 22 October 2001 / Published online: 21 January 2002

Abstract. Monte Carlo simulations have been carried out for 2-ethoxyethanol (C_2E_1) in isothermal-isobaric ensemble (NPT) at different temperatures and 1 atm pressure with a continuum configurational biased procedure in water and chloroform media. Hydrogen bond bridges were formed between adjacent oxygen atoms in C_2E_1 ($CH_3CH_2OCH_2CH_2OH$) through water molecules. We also found that the stable conformers of C_2E_1 in water and $CHCl_3$ are different and the effect of temperature on solute-solvent interaction energies is considerable. The self-association of C_2E_1 in aqueous and nonaqueous media has been studied by statistical perturbation theory, and the relative free energy has been obtained at different reaction coordinates by double-wide sampling method. Two minima were found in water solvent in the potential of mean force (PMF), corresponding to the contact and solvent-separated pairs, but only one minimum was found in $CHCl_3$ solvent corresponding to a contact pair complex.

Key words: Continuum configurational biased Monte Carlo simulation – Statistical perturbation theory – CCBMC – Ab initio calculation – 2-Ethoxyethanol

Introduction

Amphiphilic compounds (such as surfactants) have many technological applications, such as tertiary oil recovery or detergency [1]. The statistical thermodynamic description of these compounds has received considerable attention. In these studies lattice models or (continuum) mean field theories have been used to investigate the relation between the chemical structure of amphiphilic compounds and their thermodynamic properties [2]. Amphiphilic compounds consist of a hydrophilic moiety which is soluble in water and a hydrophobic moiety, which is not. This unique duality towards an aqueous environments leads to a rich spectrum of complex self-association phenomena that simpler solute molecules do not exhibit. In order to avoid contact of the hydrophobic moieties with water the individuals associate with each other to form a variety of aggregate structure [1]. Monte Carlo (MC) and Molecular Dynamic (MD) simulations [3] have been applied on some amphiphilic compounds and have shown that the results of the simulations depend on the used models [4, 5, 6, 7]. These simulations concentrate on the interfaces, e.g., oil/water interface or air/water interface [8]. Smit and coworkers perform MD simulation, showing the spontaneous formation of micelles in water in addition to the formation of monolayers of surfactants at the interface [8]. Several aqueous mixtures of polyelectrolytes and surfactants have also been investigated [9, 10]. We chose compounds belonging to the alkylpolyethylene oxide family (typically abbreviated as C_iE_j), which are widely used as detergents, solubilizers, and emulsifiers [11]. Their practical importance has triggered a significant effort to gain a fundamental understanding of their aggregation characteristics, as well as their phase behavior in both aqueous and non-aqueous media. Kong and coworkers performed MC simulations for $C_{12}E_2$ [12] and $C_{12}E_3$ [13] to investigate the perturbation of the interfacial water and the relative stability of *gauche* and *trans* chain conformations. They inserted a single chain $C_{12}E_2$ or $C_{12}E_3$ on a bilayer surface in water and by gathering radial distributions and densities for different regions in the plane of the bilayer surface examined the structure of water around the chain. The dynamical property of the molecule was lost because the most part of the molecule was fixed in the hydrocarbon walls. In their studies the SPC water potential was used.

In this work, the most stable conformers of C_2E_1 were determined by ab initio calculations at the MP2/6-31G* level. The aim of this work is to study the conforma-

Correspondence to: M. Tafazzoli
e-mail: tafazoli@sina.sharif.ac.ir

tional analysis and the association of C_2E_1 in aqueous and non-aqueous phases using the Continuum Configurational Biased MC (CCBMC) technique. In this procedure we allowed the molecule to move freely in order to vary all degrees of freedom.

Computational details

Monte Carlo simulation

The statistical mechanics calculations were carried out for computing equilibrium structural and thermodynamic features of the aqueous and non-aqueous systems via statistical mechanical averages employing standard procedures such as Metropolis sampling, periodic boundary conditions, and the isothermal-isobaric (NPT) ensemble [3, 14]. Metropolis sampling, augmented by preferential sampling, was used in which the probability of attempting to move a solvent molecule is made proportional to $1/(r^2 + C)$ where r is the central site of C_2E_1 to water oxygen distance [14–18]. The constant C was set at 89 $Å^2$, which caused the water molecules nearest the solute to be moved further as far as the most distant waters (in the $CHCl_3$ solvent C was set at 142 $Å^2$). Attempting to move the solute every 120 configurations further enhanced the solute-solvent statistics. We performed two series of simulations; the first series has been carried out in a cubic box with dimensions ca. $20 \times 20 \times 20$ $Å^3$ ($30 \times 30 \times 30$ $Å^3$ in the case of $CHCl_3$). The second series were carried out in a box with dimensions ca. $33.5 \times 22 \times 22$ $Å^3$ ($34.5 \times 31 \times 31$ $Å^3$ in the case of $CHCl_3$). The computational details are in Table 1. The external pressure was fixed at 1 atm. A spherical potential truncation at 9.5 Å and 10 Å for solvent-solvent, solvent-solute Lennard-Jones interactions are used, respectively. Analytical tail corrections (for the energy and pressure) have also been applied [3, 19]. An additional center of mass based truncation was applied for MC moves.

Consider the maximum distance of the center of mass (COM) of two molecules in the simulation box (say A and B) to any of their interaction sites to be d_A and d_B. When the COM of two molecules is more than $r_c + d_A + d_B$ and there is no direct interaction between molecules, if the cutoff distance, r_c, has been used in the simulation box. In this case, the distance between interaction sites which is less than $r_c + d_A + d_B$ could be calculated. After a successful change in the molecule conformation its maximum distance from its COM (e.g., d_A or d_B) has to be updated [20, 21].

There is an effective multiple cutoff for CBMC moves [22–25], and therefore the center of mass truncation has to be applied in a different manner. Because of growing molecules in CCBMC algorithm, there is no center of mass for molecules yet. If the distance from growing site i in molecule A to the center of mass of molecule B is more than $r_c + d_B$, then the interactions with the sites of molecule B will be ignored. Only after a successful CCBMC move need the maximum distance of center of mass to any of interaction site (d_{COM}) of the molecules be updated. In this work this cut-off was used in the CCBMC part of moves. Reaction field method was used for evaluating long-range electrostatic interactions. A detailed description of this method is given elsewhere [3, 26–30]. In addition to CCBMC moves, the range of motions for all of solute and solvent change to yield the acceptable ratio of ca. 40–50% for new conformation. In this case, new configurations were generated by randomly selecting a monomer, translating it in all three Cartesian directions, rotating it randomly about a randomly chosen axis, and performing any torsional motion. The ranges for three types of motions for solute and solvent molecules are given by $\pm\Delta r$, $\pm\Delta\theta$, and $\pm\Delta\phi$ in Table 1. The volume of the system changed every 2410 configurations within the suitable range and all intermolecular distances were scaled accordingly. There is an equilibration phase in each simulation. Equilibration should continue until the values of a set of monitored properties become stable. The energy of the system, including solvent-solvent and solvent-solute interactions, has been selected as an equilibration criterion. In each simulation the generated configurations of equilibration was discarded and averaging was performed over configurations generated in the sampling simulations. The initial configuration for the first simulation was obtained from an equilibrated solvent box. In this work a configurational bias move and a volume displacement were carried out simultaneously as recommended by de Pablo et al. [31]. (As the size of the chain increases, the amount of CCB move increases.)

All geometry optimizations in the gas phase and single point energy evaluations were performed with the GAUSSIAN 94 program [32].

Continuum Configurational Biased Monte Carlo (CCBMC)

Monte Carlo simulations of flexible molecules are often difficult to perform successfully unless the system is

Table 1. Computational details for MC simulations

Series	# Water (chloroform)	# C_2E_1	$\pm\Delta r$ (Å)[a]	$\pm\Delta\theta$ (deg)	$\pm\Delta\phi$ (deg)[b]	$\pm\Delta V$ ($Å^3$)	No. of config ($\times 10^{-6}$)[c]
First	260 (200)	1	0.17 (0.18)	15 (18)	15	570	1.7 (4.7)
Second	540 (256)	2	0.17 (0.18)	15 (18)	15	610	1.7 (5.2)

[a] $\pm\Delta r$, $\pm\Delta\theta$ and $\pm\Delta\phi$ are the ranges of translating, rotating, and torsional motions, respectively. $\pm\Delta V$ is the volume change. The values in parenthesis related to the solvent

[b] Used in simulations without CCBMC part for modifying Lennard-Jones parameters

[c] The first value is for equilibration and the value in parenthesis is for sampling

small/some of the internal degrees of freedom are frozen out/special models or methods are employed. The simplest way to generate a new configuration of a flexible molecule is to perform random changes to the Cartesian coordinates of individual atoms, in addition to translations and rotations of the entire molecule. Unfortunately, it is often found that a little atomic displacement is required to achieve an acceptable ratio, which means that the configuration space is covered very slowly. One obvious tactic is to freeze out some of the internal degrees of freedom, usually the "hard" degrees of freedom such as the bond lengths and bond angles. The rigid bond length and rigid bond angle approximations must be used with care for freezing out some of the internal degrees of freedom, which can affect the distributions of other internal degrees of freedom [33]. The configurational-bias method has circumvented some of the sampling problems encountered for complicated potentials and chain molecules. This method is based on growing the chains in a dense fluid in a manner that looks for available space, thereby increasing the likelihood of generating low-energy configurations.

CCBMC draws upon ideas originated by Rosenbluth and Rosenbluth [34]. Use of this technique makes it possible to achieve a large-scale change in the conformation of a flexible molecule in the course of a single MC move [35]. In summary, the continuum configurational bias (CCB) Monte Carlo (MC) method consists of three steps. The first step is cutting off one end of the chain (randomly) at a random point. The second step is regrowing the chain segment by segment. In this case each segment has a continuum of dihedral angles (0 to 2π) to choose from. A suitable method for calculation of Rosenbluth weight for placing of segments is discretizing this interval uniformly [31]. There is n_{choice} positions available for each segment. The number of angles sampled while placing an individual segment (n_{choice}) has selected eight, that is, angle distribution has uniformly been discretized in intervals of 45°. The rotational angle for each appended segment is chosen with the probability dictated by Eq. (1):

$$w_i = \frac{w_i}{\sum_j w_j} \tag{1}$$

in which w_i is the Boltzmann weight of position i.

The third step is accepting or rejecting the trial chain configuration according to an importance-sampling criterion. Clearly, trial configurations are generated with a bias that favors low-energy configurations on a segment-by-segment basis. This bias is subsequently removed by accepting or rejecting the proposed trial configuration with probability [36, 37]

$$P_{CCB} = \min(1, W_{old}P_{new}/W_{new}P_{old}) \tag{2}$$

where W_{new} and W_{old} are the probabilities of generating the new (trial) and old (previously accepted) chains, respectively, and P_{new}/P_{old} is the ratio of the probabilities of the new and old configurations of the system. By accepting or rejecting trial configurations according to Eq. (2), a series of structures distributed according to an equilibrium distribution function are generated.

Intermolecular potential functions

The general form of intermolecular functions including Coulomb and Lennard-Jones between interaction sites i and j on the two molecules a and b is [38, 39]

$$V_{ab} = \sum_i^a \sum_j^b \left(q_i q_j e^2 / r_{ij} + A_{ij}/r_{ij}^{12} - C_{ij}/r_{ij}^6 \right) \tag{3}$$

Standard combining rules are used as follows: $A_{ij} = (A_{ii}A_{jj})^{1/2}$ and $C_{ij} = (C_{ii}C_{jj})^{1/2}$. The A and C parameters may also be expressed in terms of Lennard-Jones εs and σs as $A_{ii} = 4\varepsilon_i\sigma_i^{12}$ and $C_{ii} = 4\varepsilon_i\sigma_i^6$. The four-site TIP4P model for water was used in conjunction with OPLS potential (Table 2). For C_2E_1 the CH_2 and CH_3 groups on the chain atoms were modeled as united atoms (sites) and the hydroxyl oxygen and hydrogen as discrete sites. The C_2E_1 was modeled using Optimized Potential for Liquid Simulations (OPLS) molecular force field parameters. The OPLS parameters for C_2E_1 (Table 2) are taken from the literature [40] and modified for our calculations (Table 2). A series of short liquid simulations have been carried out for C_2E_1 for examining the OPLS parameters and the key points of comparison with experimental data were the heat of vaporization and density of liquid C_2E_1. The obtained density from liquid simulation was 0.914 g cm^{-3}, which is in agreement with experimental value (0.903 g cm^{-3}) [41].

Torsional motion about CO, OC, CC and CO bonds in C_2E_1 was included in all simulations. The Fourier series (Eq. 4) describes the rotational potential energy about each bond [29, 42]:

$$V(\varphi) = \frac{V_1}{2}(1 + \cos(\varphi)) + \frac{V_2}{2}(1 - \cos(2\varphi)) + \frac{V_3}{2}(1 + \cos(3\varphi)) \tag{4}$$

For C_2E_1 molecule the Fourier series needs to be augmented by 1,5-Lennard-Jones potential as follows:

$$V(\phi, r) = \sum_{i=1}^{3} V(\phi_i) + \sum_{i<j}^{>1,4} \left(A_{ij}/r_{ij}^{12} - C_{ij}/r_{ij}^6 \right) \tag{5}$$

General parameters were developed for C_2E_1 by fitting to RHF/6-31G* ab initio energies for 74 conformers of C_2E_1. In general, use of RHF/6-31G* or higher level of ab initio quantum mechanical calculations is a well-accepted procedure for calculation of torsional parameters [43–45]. The Fourier coefficients in Table 3 give the best results in agreement with experimental data [heat of vaporization (ΔH_{vap}) and densities (Table 4)]. In fitting by nonlinear least-squares regression the Fourier coefficients and Lennard-Jones parameters were coupled. After several tests of the fitting process, we decided to use the values listed in Table 5. An approximation value for the heat of vaporization is computed from Eq. (6) [14, 40]:

$$\Delta H_{vap} = E_{\text{int}\,ra}(g) - (E_i(1) + E_{\text{int}\,ra}(1)) + RT \tag{6}$$

where the intramolecular rotational energy for the gas may be obtained from a Boltzmann distribution

for V (ϕ, r). This method is applicable to molecules with only one or two dihedral angles. However, for C_2E_1, with four dihedral angles, $E_{\text{int ra}}(g)$ was determined from a CCBMC simulation of an isolated C_2E_1 molecule.

A utility was added to our own program to performing CCBMC simulations [26, 46, 47].

Statistical mechanical calculations

The potential of mean forces (PMF) for association of C_2E_1 in aqueous and chloroform ($CHCl_3$) media were determined by using statistical perturbation theory (SPT). One of the possibilities of calculating Gibbs free energy of association is based on SPT from which [48, 49]

$$\Delta G_{BA} = -k_B T \ln[\exp(-\beta \Delta E_{BA})]_A \quad (7)$$

where k_B is the Boltzman constant, T the absolute temperature, and $\beta = (k_B T)^{-1}$. ΔE_{BA} denotes the difference in energy between the two systems A and B at a given configuration, and $[\ldots]_A$ denotes the ensemble

Table 2. OPLS parameters for C_2E_1, water and chloroform

	ε (kcal mol^{-1})	σ (Å)	q (e)
C_2E_1[a]			
CH_3	0.175	3.905	0.0000
CH_2	0.207	3.775	0.270
O	0.817	3.047	−0.580
CH_2	0.478	3.983	0.290
CH_2	0.748	3.983	0.290
O	0.467	3.070	−0.700
H	0.000	0.000	0.435
H_2O			
O	0.155	3.154	0.000
H	0.000	0.0000	0.52
M[b]	0.000	0.0000	−1.040
$CHCl_3$			
C	0.071	3.602	−0.091
H	0.038	2.500	0.098
Cl	0.300	3.470	−0.203

[a] The Lennard-Jones parameters for CH3, Os, and H of C2E1 are modified
[b] M is a point on bisector of the HOH angle, 0.15 Å from the oxygen toward the hydrogens

Table 3. Fourier coefficients for intramolecular rotational potential function

Dihedral angle	V_1[a]	V_2	V_3
C1C2O3C4 (Φ_1)	4.746	−1.401	2.143
C2O3C4C5 (Φ_2)	4.746	−1.401	2.143
O3C4C5O6 (Φ_3)	0.703	−0.213	3.064
C4C5O6H7 (Φ_4)	0.834	−0.116	0.748

[a] Units for the Vs are kcal mol^{-1}

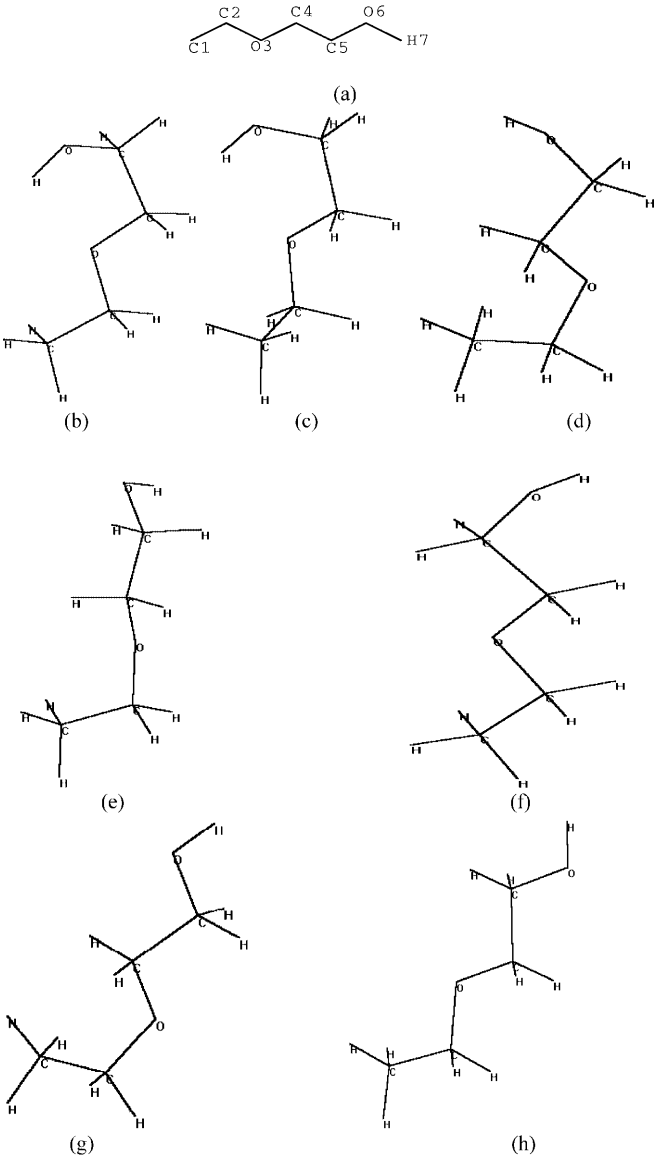

Fig. 1a–h. The most stable conformations of C_2E_1 in gas phase and numbering of atoms for C_2E_1. Numbering of atoms in: **a** C_2E_1; **b** ttGg$'$; **c** gtGg$'$; **d** gtTg$'$; **e** gtTg; **f** ttTg; **g** gtTt; **h** ttTt

Table 4. Densities and enthalpy of vaporizations for C_2E_1, $CHCl_3$, and H_2O

Compound	Density[a] (experimental)	Density (calculated)	ΔH_{vap}[b] (experimental)	ΔH_{vap} (calculated)
C_2E_1	0.90300	0.914 ± 0.007 (0.918 ± 0.007)[c]	10.77	10.61 ± 0.07
$CHCl_3$	1.47300	1.471 ± 0.005	7.48	7.51 ± 0.05
H_2O	0.99821	0.999 ± 0.004	10.51	10.50 ± 0.03

[a] Densities in g cm^{-3} and experimental data taken from [41]
[b] Enthalpies (heat of vaporizations) in kcal/mol and experimental data from [41]
[c] The value in parenthesis calculated from conventional MC method the other calculated from CCBMC method

average corresponding to system A. In MC simulation, the ensemble average is approximated by a set of sampled configurations. Since sampling is performed for system A, it must be ensured that the set of generated configurations includes a set of configurations representing state B. If state A and B do not overlap in phase space, then the value of calculated free energy differences will not be very accurate, because we have not adequately sampled the phase space of B when simulating A. If the two states A and B differ strongly, ΔE_{BA} will be generally very large, and the simulation period needed to converge Eq. (7) will exceed the computationally feasible period. In this case, the perturbation may be split into n smaller increments, so-called windows; for each of these the free energy differences can be determined individually as follows (Eq. 8) [49]:

$$\Delta G_{BA} = \sum_{i=0}^{n-1} \Delta G_{i \to i+1} \tag{8}$$

in which

$$\Delta G_{i \to i+1} = -k_B T \ln[\exp(-\beta \Delta E_i)]_i \tag{9}$$

where n is the number of windows, and $\Delta E_i = E_{i+1} - E_i$. Sampling at intermediate system i enables us to calculate the free energy differences to the $i + 1$ and $i - 1$ systems. Hence, one simulation allows the simultaneous calculation of two free energy differences. This technique is called "double-wide" sampling. The total free energy is obtained from these two values. In this work the reaction coordinate (r_c) was chosen as the distance

Table 5. Accepted values for 1,5-nonbonded interactions in C_2E_1 molecule

	σ (Å)	ε (kcal mol^{-1})
$C_1 \cdots C_5$	4.000	0.00075
$C_2 \cdots O_6$	3.143	0.0095
$O_3 \cdots H$	2.890	0.0100

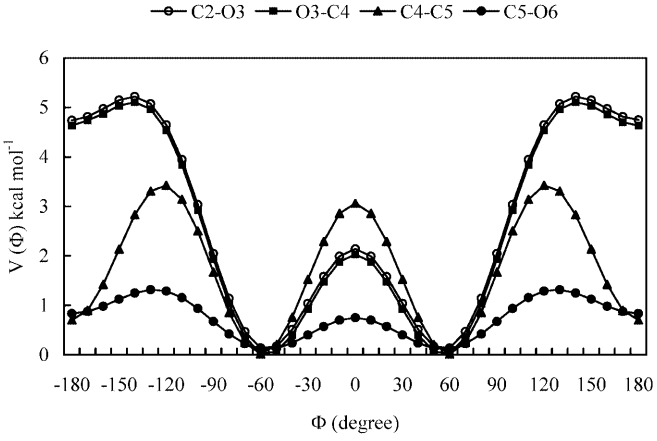

Fig. 2. potential function (kcal mol^{-1}) for rotation about the different bonds in C_2E_1

Table 6. Relevant MP2/6-31G* results 1, for the more stable conformers of C_2E_1 (the value of dihedrals for each conformation are in degrees and are written as footnotes. The value are for Φ_1, Φ_2, Φ_3, and Φ_4, respectively)

Conformer	ttGg[a]	gtGg[b]	gtTg[c]	gtTg[d]	ttTg[e]	gtTt[f]	ttTt[g]
E/E_{HF}[h]	−306.9914	−306.9888	−306.9854	−306.9853	−306.9879	−306.9878	−306.9883
μ/D[j]	2.846	2.870	2.281	2.485	2.312	0.408	0.435
Bond lengths[i]							
C1C2	1.5134	1.5020	1.5208	1.5209	1.5136	1.5210	1.5137
C2O3	1.4249	1.4297	1.4261	1.4263	1.4232	1.4256	1.4227
O3C4	1.4249	1.4263	1.4191	1.4188	1.4174	1.4203	1.4190
C4C5	1.5132	1.5133	1.5190	1.5189	1.5184	1.5132	1.5128
C5O6	1.4215	1.4214	1.4271	1.4271	1.4272	1.4275	1.4273
O6H7	0.9744	0.9744	0.9716	0.9715	0.9716	0.9708	0.9708
Bond angles[h]							
C1C2O3	107.7101	112.54	113.1505	113.1485	107.6894	113.1797	107.6749
C2O3C4	112.6105	113.65	113.6077	113.5995	112.1589	113.3977	111.9538
O3C4C5	105.6887	105.4415	106.9359	106.9191	107.3569	106.5847	106.9807
C4C56	110.3696	110.3291	111.2066	111.1999	111.1833	106.3152	106.3063
C5O6H7	104.5629	104.4997	107.2681	107.2706	107.2724	107.6333	107.6388
Non-bonded atom distances[h]							
O3···O6(−H7)	2.743	2.746	3.636	3.635	3.638	3.583	3.585
O3···H7(−O6)	2.237	2.243	3.912	3.926	3.920	4.290	4.294

[a] −179, −179, 60, −50 (Φ_1 = C1C2-O3C4, Φ_2 = C2O3-C4C5, Φ_3 = O3C4-C5O6, Φ_4 = C4C5-O6H7)
[b] 80, 180, 60, −50
[c] 70, 170, 169, −65
[d] 70, 170, 169, 66
[e] −179, −179, 180, 72
[f] 70, 170, 170, 180
[g] 180, 180, 180, 180
[h] Energies are in hartrees (one hartree is 627.51 kcal mol^{-1}
[i] Bond lengths are in Å, bond angles are in degree and non-bonded distances are in Å
[j] D(= Debye) = 3.33564×10^{-30} C.m. (C = coulomb)

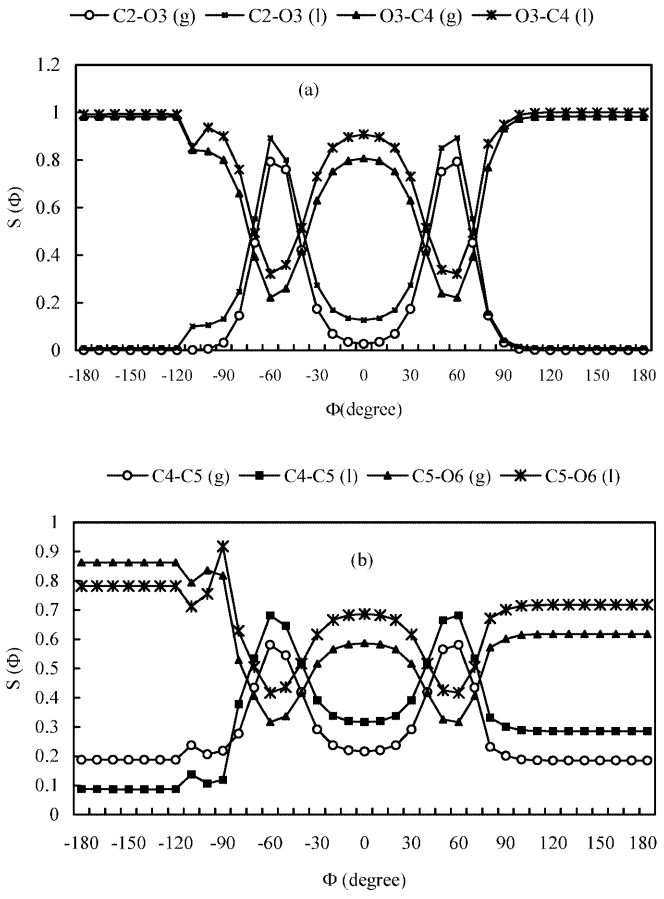

Fig. 3. Population distribution for important dihedral angles of C_2E_1. Units for s (ϕ) are mole fraction per degree (g = gas phase, l = liquid phase)

Table 7. Average coulombic and Lennard-Jones solute-solvent energy contributions from the MC simulations at different temperatures in water and chloroform solvents

	$[U_{vdw}]^a$	$[U_{elec}]$
H_2O		
298.15[b]	−16.6 ± 0.2	−29.0 ± 0.4
343.15	−15.4 ± 0.2	−24.9 ± 0.3
353.15	−15.5 ± 0.3	−25.8 ± 0.2
	−15.4 ± 0.3	−24.1 ± 0.6
HCl_3		
298.15	−30.9 ± 0.6	−1.9 ± 0.6
343.15	−27.3 ± 0.7	−1.8 ± 0.5
353.15	−26.8 ± 0.6	−1.7 ± 0.3
363.15	−26.0 ± 0.5	−1.9 ± 0.6

[a] Units for energies are kcal mol^{-1}
[b] Units for temperatures are Kelvin (K)

between the C3 sites (central site) in two C_2E_1, and the SPT has been used by sequentially perturbing along the reaction coordinate in steps of 0.2 Å (each center moved in or out by 0.1 Å). The uncertainties in the incremental ΔG values ($\pm 1\sigma$) were obtained by the batch means procedure [3]. For each value of the reaction coordinate a full simulation has been carried out. For obtaining the PMFs of C_2E_1 it is necessary to calculate the interaction energies among solutes and between solutes and water molecules at each r_c [50, 51]. It also worth noting that only relative free energy values may be calculated and the resulting potential of mean force must be normalized. Subsequently, the PMFs are obtained by joining the results of each simulation at the end point.

Results and discussion

Figure 1 represents the more stable conformations of C_2E_1 in the gas phase and numbering of the atoms involves. For the identification of the atoms in structural parameters and whenever ambiguity does not occur, the number of atoms is omitted and the order of numbering is the same as Fig. 1a. We use the symbol t or T (*trans*), g or G (+*gauche*), and g′ or G′ (−*gauche*) to describe the arrangement of groups around each dihedral. The optimized geometries of C_2E_1 are identified by a four-letter acronym specifying the C1C2O3C4 (lower case), C2O3C4C5 (lower case), O3C4C5O6 (upper case), and C4C5O6H7 (lower case) axes as *trans* (t, T), +*gauche* (g, G), or −*gauche* (g′, G′) arrangements, e.g., ttGg′ and ttTg. Table 6 presents the relative conformational energies, dipole moments, and the most relevant optimized

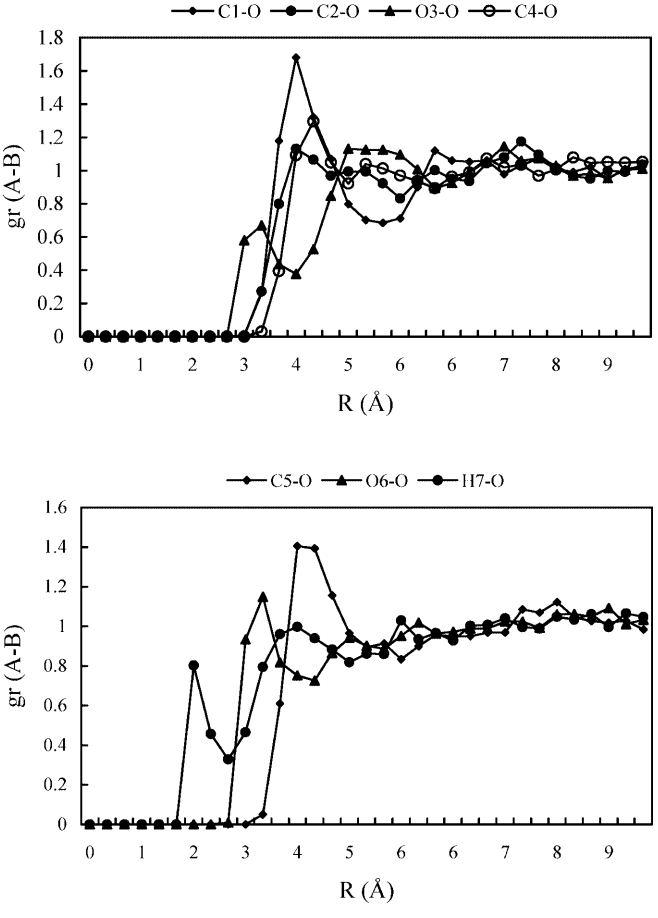

Fig. 4. Computed A_n (C_2E_1)-O (water) rdfs for solute C_2E_1 in water at 298.15 K. (A_n is the n-th atom of C_2E_1)

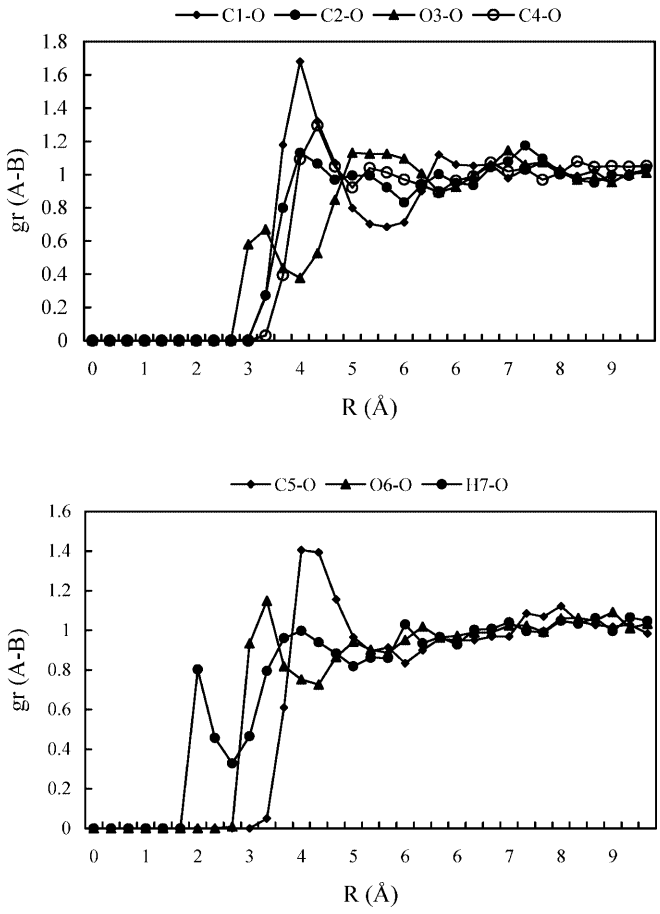

Fig. 5. Computed A_n (C_2E_1)-H (water) rdfs for solute C_2E_1 in water at 298.15 K. (A_n is the n-th atom of C_2E_1)

structural parameters for the more stable conformers in the gaseous phase calculated at the MP2/6-31G* ab initio level. The gtGg/ and ttGg/ are the most stable conformers. By considering the short non-bonded atom O3···O6(-H7) and O3···H7(-O6), distances indicate the occurrence of intramolecular hydrogen bonds in gtGg/ and ttGg/ conformers, between the ether O3 atom and the hydroxyl H7 atom. These intramolecular interactions seem to be decisive to explain the stability of these conformers, since the lack of hydrogen bonds in other G-type conformers caused less stability. Table 6 also shows that by, increasing the non-bonded distances, the stability of conformers decrease. In C_2E_1 molecule the dipole moment changed extensively by varying the dihedral angles (Table 6). This indicates that the charge distribution changes with internal degrees of freedom, which depends on the electric field from other parts of the molecule.

Particular care was given to the intramolecular potential due to its influence on the relative stability of *trans* and *gauche* forms. The computed intramolecular rotational energies and full dihedral angle distributions, S(ϕ), for the liquid phase and corresponding gaseous phase are shown in Figs. 2 and 3. The dashed curves are the ideal gas results for S(ϕ) derived from Boltzman distribution for V(ϕ). The results for ϕ_1 and ϕ_2 in C_2E_1 are essentially similar; the percent of +g and −g is also similar for each and is due to their nearly identical environments. Most of the variations in structure and relative energies are due to the complex interplay between the torsional and non-bonded contributions. For C_2E_1, by rotation around C2-O3 there are two energy minima for *trans* conformations and three maxima for structural conformations (Fig. 2). The antibonding interactions are minimized when conformation is *gauche* and are at a maximum at −180°, 0°, and 180° of ϕ_1 angles. The energy profile for rotation about a bond that is described by a general torsional potential depends solely upon the atom type of the two atoms that comprise the central bond, and not upon the atom types of the terminal atoms. As we can see in Fig. 2, the rotational energies profile for C2-O3 and O3-C4 are similar, and it is expected that they be assigned the same torsional parameters. For describing the rotational energy we used Eq. (4) whereby for each of the three terms a physical interpretation has been ascribed, for each substance. By rotation around C4-C5 bond there are the two minima at 60° and −60° corresponding to *gauche* conformers and also three sharp maxima were produced with *trans-gauche* barriers larger than the others. Dihedral angle distributions for C_2E_1 are shown in Fig. 3. The principal conclusion resulting from these figures is that the condensed phase environment has a significant effect on the conformational equilibrium for C_2E_1. It appears that the ϕ_3 dihedral angle has a slightly higher *trans* population in both liquid and gas phases than the other angles. For each dihedral the population of *gauche* conformer is higher than other conformers, which perhaps is due to the more effective intramolecular interactions in *gauche* conformers, e.g., intramolecular hydrogen bond.

We have performed two series of MC simulations in water and $CHCl_3$ in order to study the effects of solvent and temperature on the conformational structure of C_2E_1. The intermolecular interactions have been divided in two parts; Lennard-Jones contribution (Van der Waals interaction) and Coulombic (electrostatic) contribution. Our program [26, 46, 47] was modified to calculate the separate components of the solute-solvent interaction energies. Thus the intermolecular interactions could be written as follows [46, 52]:

$$\Delta E_{ab}=\sum_i\sum_j\left\{\frac{q_iq_je^2}{r_{ij}}\right\}+\sum_i\sum_j\left\{4\varepsilon_{ij}\left[\left(\frac{\sigma_{ij}}{r_{ij}}\right)^{12}-\left(\frac{\sigma_{ij}}{r_{ij}}\right)^{6}\right]\right\} \tag{10}$$

$$\Delta E_{ab} = U_{elec} + U_{vdw} \tag{11}$$

where $\varepsilon_{ij} = \sqrt{\varepsilon_i\varepsilon_j}$.

The values of these components are represented in Table 7. Comparing the results of this table showed that the Van der Waals (vdw) interaction contributions for $CHCl_3$ are larger than for water, but the electrostatic interaction for water is larger than $CHCl_3$, and this can be related to the polarity of solvents. By increasing temperature the U_{vdw} and U_{elec} become more positive

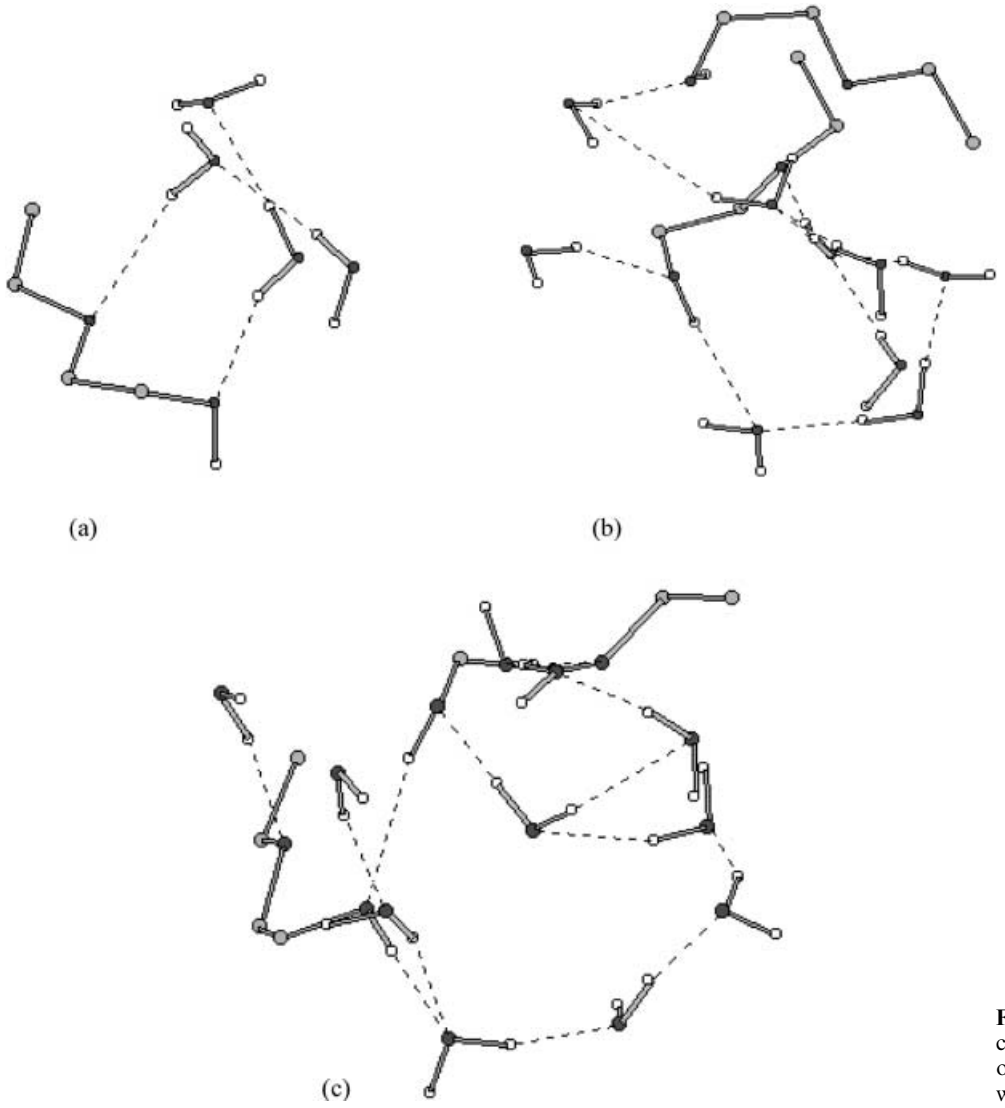

Fig. 6a–c. Stereoplot of different configurations from the simulation of C_2E_1 in water: **a** single C_2E_1 in water; **b** $r_c = 3.6$ Å; **c** $r_c = 6.2$ Å

with almost regular trends for the two solvents. This means that the intermolecular interactions decrease with increasing temperature due to increasing thermal motion of the molecules. The effect of temperature on U_{elec} in $CHCl_3$ does not show a regular trend.

The presence of hydrogen bonds was monitored for coordinates saved every 4×10^4 configurations during the simulation by using defined criteria [53]. The formation of hydrogen bonds can be indicated by either geometrical criteria or energy criteria, when the distance of O···H in molecule is less than 2.5 Å and/or the interaction energy of molecules is not more positive than -2.25 kcal mol^{-1} respectively. The formation of hydrogen bonds between water and C_2E_1 molecules have been studied and it is found that the average number of hydrogen bonds between solute and solvent is 2.6 and the average energy is -6.229 kcal mol^{-1}.

More information could be obtained about the arrangement of water in the vicinity of the chain by studying water-chain radial distribution functions (rdfs). The rdfs for C_2E_1 water sites are shown in Figs. 4 and 5. The first sharp peak for H7-O (Fig. 4) occurred at 1.95 Å, at smaller distance from the peaks of other rdfs. This seems reasonable because H7 is the most exposed and has an efficient interaction with water O atom. The second peak of the H7-O rdf occurred at 4.05 Å. The nearest neighbor separation for O6 and O3 with water O is ca. 3.15 Å, where the height of O6-O (1.149) is higher than the height of O3-O (0.67) and it is a remarkable achievement. The first peak of the C–O rdfs occurred at 3.75–4.05 Å, with a sharp peak for C1-O. In Fig. 5 regular trends were found for all rdfs. The first peak of H7-H is located at 2.1 Å. The second peak of H7-H, at 4.7 Å, is wider than the second peaks of the other rdfs. The first peaks of O6-H and O3-H are located at 2.9 Å and the first peak of O6-H is wider than O3-H, and it is probably due to the less hindrance around O6. The first peak of the C-H rdfs is located at 3.7–4 Å. The C1-H peak is higher than the others, which is reasonable.

When the solute molecule is surrounded by water molecules, they tend to form hydrogen bond bridges between adjacent O atoms in a C_2E_1 molecule, and this stabilizes the obtained conformation which is like ttGg$^{/}$. Figure 6 shows this feature. In $CHCl_3$ the stable conformers are different from those in water, which are all in *trans* form (Fig. 7).

The association of C_2E_1 in water and $CHCl_3$ has been studied by performing a series of MC simulations. In these simulations the distance between central sites in two C_2E_1 molecules was considered as a reaction coordinate, r_c. MC simulations were performed to span the r_c range from 3 to 9 Å to obtain the potential of mean force of C_2E_1, where in each simulation the relative free energy was obtained for each solvent. The results of these calculations are represented in Figs. 8 and 9. The PMF plot of C_2E_1 in water shows two minima for association of C_2E_1. The first minimum in water solvent is due to a contact pair complex in which no water molecule separates two solutes and so the solute molecules contact each other. In the other minimum the solute molecules are separated by one or more water molecules. The separating maximum can be interpreted as a barrier for the transition from C_2E_1-C_2E_1 to C_2E_1–(H_2O)-C_2E_1, where the first is the contact pair and the second is the solvent separated complex. Although for the second complex there is a hydrogen bond between water and two solute molecules, it has slightly higher energy than the first complex. Calculation of relative probability by Eq. (12) and integration over each minimum show that the first complex is more probable than the second one:

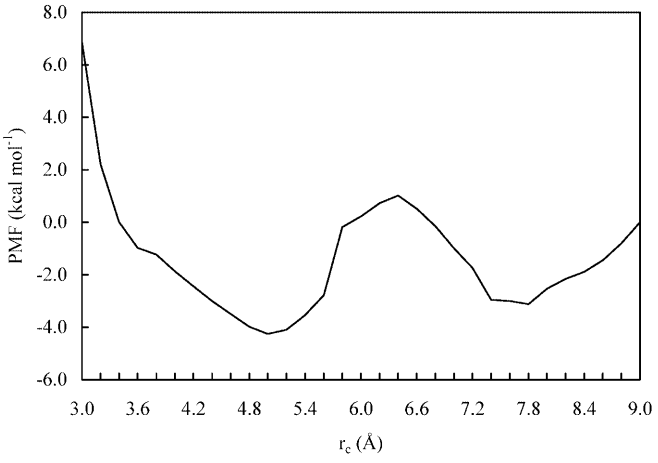

Fig. 8. Potential of mean force (PMF) for self-association of C_2E_1 in water

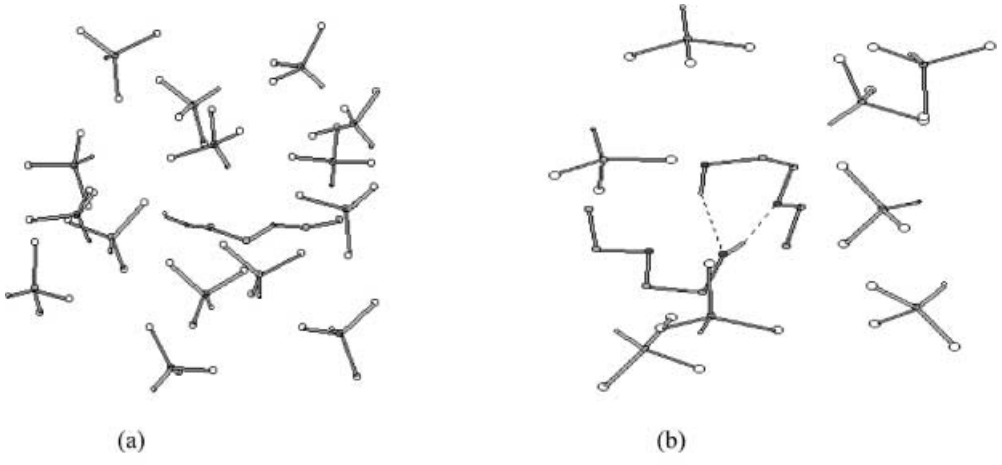

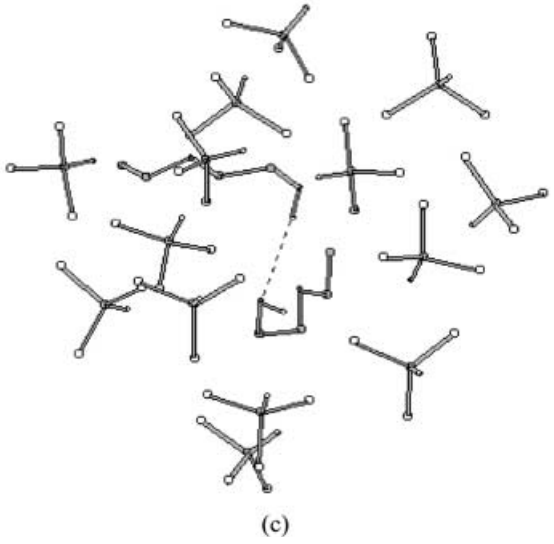

Fig. 7a–c. Stereoplot of different configurations from the simulation of C_2E_1 in $CHCl_3$: **a** single C_2E_1 in $CHCl_3$; **b** $r_c = 3.6$ Å; **c** $r_c = 6.2$ Å

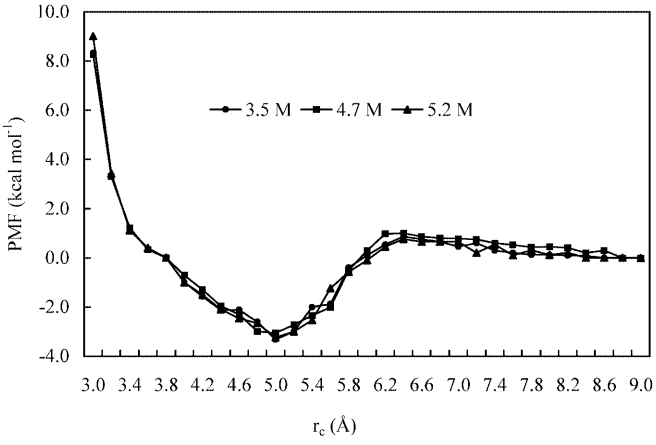

Fig. 9. Potential of mean force (PMF) for self-association of C_2E_1 in $CHCl_3$ in the averaging period from 3.5 to 5.2 million configurations

$$P(r) = 4\pi r^2 \exp\left(-\frac{W(r)}{k_B T}\right) \quad (12)$$

in which W(r) is PMF at reaction coordinate r. We think the greater stability of the first complex is due to the greater tendency of these compounds for aggregation in aqueous media. The PMF for association of C_2E_1 in $CHCl_3$ shows only one minimum, corresponding to contact pair complex. To check the reliability of the PMF results in $CHCl_3$ solvent, the convergence of the PMF was investigated in more detail. It is found that extending the averaging period from 3.5 to 5.2 million configurations has little effect on the result.

One of the most useful ways to investigate the association phenomena is to explore spatial views of different configurations. Figure 6 shows a spatial view of water molecules, which form hydrogen bonds with C_2E_1 at different values of r_c. As is shown, the hydrogen bond formation is mainly between the C_2E_1 molecules and the solvent molecules or between C_2E_1 molecules and there are no intramolecular hydrogen bonds in C_2E_1. In the PMF for association of C_2E_1 in $CHCl_3$ there is only one minimum which is due to the formation of a contact pair of solute in $CHCl_3$ solvent. The views of Fig. 7 reveal that the formation of a hydrogen bond between two solutes in $CHCl_3$ is more effective than in water. These views have been obtained by considering only the nearest solvent molecules around the solute. Inspection of these views shows that the two oxygens in C_2E_1 formed a hydrogen bond with an H atom from the other molecule and a large cage has been formed between the two solutes. There are no solvent molecules in this cavity. The largeness of the molecule and lower polarity of $CHCl_3$ may be the cause of this arrangement. The formation of this cavity has been observed in all reaction coordinates. A noticeable point is the conformation of C_2E_1 in $CHCl_3$ in the two series of simulations (one solute and two solutes in solvent). In the case of two solutes (C_2E_1) the curved conformation is predominant but in the case of one solute molecule in solvent the straight conformation is predominant.

Conclusions

2-Ethoxyethanol has been found to form an internal hydrogen bond in gaseous phase while in solution the water molecules form hydrogen bonds between adjacent O atoms in the C_2E_1 and stabilize the conformers in aqueous solvent. In non-aqueous solvent ($CHCl_3$) the stable conformers are different from aqueous solvent. It is found that straight conformers are more stable than others in water. By applying Monte Carlo simulations it was found that in the condensed-phase the dihedral populations differ from gas phase. The water molecules accumulate around C_2E_1 molecules and form hydrogen-bonded bridges between adjacent O atoms in the solute molecule. The effect of temperature on the solute-solvent interaction energy is considerable in both solvents. By increasing temperature the Van der Waals interaction become more positive and in $CHCl_3$ this trend is severe. The electrostatic interaction has the same trend as the Van der Waals interaction. The U_{vdw} in $CHCl_3$ is more negative than U_{elec}, while in water the U_{elec} is more negative than U_{vdw}. The free energy profiles for C_2E_1 in water showed two minima (at $r_c = 5.2$ and 7.8 Å) corresponding to contact and solvent-separated pairs. The maximum separating these two positions can be interpreted as a barrier to the transition from C_2E_1-C_2E_1 to C_2E_1 – (H_2O)-C_2E_1. The tendency to form hydrogen bond bridges by water is more effective than internal hydrogen bonds for longer r_c values. This showed that formation of such bridges could be an effective driving force for the association of hydrophilic groups. The association of C_2E_1 in $CHCl_3$ has only one minimum at $r_c = 5.2$ Å, corresponding to the contact pair complex.

References

1. Mitall KL, Lindman B (1984) Surfactants in solutions. Plenum, New York
2. Allen MP, Tildesley DJ (1993) Computer simulation in chemical physics. Kluwer Academic Publisher, The Netherlands, chap 12, p 461
3. Allen MP, Tildesley DJ (1987) Computer simulation of liquids. Oxford University Press
4. Gruen DWR (1985) J Phys Chem 89: 153
5. MacKerell AD Jr (1995) J Phys Chem 99: 1846
6. Schweigofer KJ, Essmann U, Berkowitz M (1997) J Phys Chem B 101: 3793
7. Tarek M, Tobias DJ, Klein ML (1995) J Phys Chem 99: 1393
8. Smit B, Hilbers PAJ, Esselink K, Rupert LAM, Van Os NM, Schlijper AG (1991) J Phys Chem 95:6361
9. Hautman J, Bareman JP, Mar W, Klein ML (1991) J Chem Soc Faraday Trans 87: 2031
10. Nuzzo RG, Allara DL (1983) J Am Chem Soc 105: 4481
11. Van Os NM, Aak JR, Rupert LAM (1993) Physico-chemical properties of selected anionic, cathionic and nonionic surfactants. Elsevier Science Publisher B.V., chap III.1
12. Kong YC, Nicholson D, Parsonage NG, Thompson L (1994) J Chem Soc Faraday Trans 90: 2375
13. Kong YC, Nicholson D, Parsonage NG (1995) J Chem Soc Faraday Trans 91: 4261
14. Lykos P (1978) Computer modeling of matter. American Chemical Society, USA, pp 159–171; Owicki JC, Scheraga HA (1977) Chem Phys Lett, 47: 600

15. Jorgensen WL, Madura JD, Swensen CJ (1984) J Am Chem Soc 106: 6638
16. Jorgensen WL, Swensen CJ (1985) J Am Chem Soc 107: 569
17. Jorgensen WL (1986) J Phys Chem 90: 1276
18. Jorgensen WL, Swensen CJ (1985) J Am Chem Soc 107: 1489
19. Wood WW, Parker FR (1955) J Chem Phys 27: 720
20. Martin MG, Siepmann JI (1998) J Phys Chem B 102: 2569
21. Martin MG, Siepmann JI (1998) Theor Chem Acc 99: 347
22. Vlugt TJH, Martin MG, Siepmann JI (1998) Mol Phys 94: 727
23. Wick CD, Martin MG, Siepmann JI (2000) J Phys Chem B 104: 8008
24. Martin MG, Siepmann JI (1999) J Phys Chem B 103: 4508
25. Barker JA, Watts RO (1973) Mol Phys 26: 789
26. Tafazzoli M, Jalili S (2001) J Mol Liquids 89: 19
27. Onsager L (1936) J Am Chem Soc 58: 1486
28. Kirkwood JG (1939) J Chem Phys 7: 911
29. Essex JW, Jorgensen WL (1995) J Phys Chem 99: 17,956
30. Barker JA (1980) Reaction field method for polar fluids. In: Ceperly D (ed) The problem of long-range forces in the computer simulation of condensed matter. NRCC, Workshop proceedings, vol 9, pp 45–46
31. de Pablo JJ, Laso M, Suter UW (1992) J Chem Phys 96: 2395
32. Frisch MJ, Trucks GW, Schlegel HB, Gill PMW, Johnson BG, Robb MA, Cheeseman JR, Keith T, Petersson GA, Montgomery JA, Raghavachari K, Al-Laham MA, Zakrzewski VG, Ortiz JV, Foresman JB, Peng CY, Ayala PY, Chen W, Wong MW, Andres JL, Replogle ES, Gomperts R, Martin RL, Fox DJ, Binkley JS, Defrees DJ, Baker J, Stewart JP, Head-Gordon M, Gonzalez C, Pople JA, (1995) Gaussian 94, Rev B.2, Gaussian Inc., Pittsburgh PA
33. Theodorov DW, Suter UW (1985) Macromolecules 18: 1467; Gusev AA, Suter UW (1991) Phys Rev A 43: 6488
34. Rosenbluth MN, Rosenbluth AW (1955) J Chem Phys 23: 356
35. Panagiotopoulos AZ (1996) Fluid Phase Equil 116: 257
36. de Pablo JJ, Laso M, Suter UW (1992) J Chem Phys 96: 6157
37. Siepmann JI, McDonald IR (1993) Mol Phys 79: 457
38. Jorgensen WL, Chadraskhor J, Madura RW, Klein ML (1983) J Chem Phys 79: 926
39. Jorgensen WL, Tirado-Rives J (1988) J Am Chem Soc 110: 1657
40. Jorgensen WL (1981) J Am Chem Soc 103: 335
41. Lide DR (ed) (1997) CRC handbook of chemistry and physics. CRC press
42. Jorgensen WL (1983) J Phys Chem 87: 5304
43. Rizzo RC, Jorgensen WL (1999) J Am Chem Soc 121: 4827
44. Jorgensen WL, Maxwell DS, Tirado-Rives J (1996) J Am Chem Soc 118: 11,225
45. Damm W, Frontera A, Tirado-Rives J, Jorgensen WL (1997) J Comput Chem 18: 1955
46. Tafazzoli M, Jalili S (2000) Chem Phys Lett 331: 235
47. Tafazzoli M, Jalili S (2001) Theor Chem Acc 106: 194
48. Wanzig RJ (1954) Chem Phys 22: 1420
49. Leach AR (1996) Molecular modeling: principles and applications. Weseley Langmon, chap 9
50. Dang LX, Kollman PA (1990) J Am Chem Soc 112: 503
51. Tobias DJ, Brooks CL III (1987) Chem Phys Lett 142: 472
52. Carlson HA, Jorgensen WL (1995) J Phys Chem 99: 10,667
53. Duffy EM, Kowalczyk PJ, Jorgensen WL (1993) J Am Chem Soc 115: 9271